Desalination and Water Treatment
www.deswater.com

doi:10.5004/dwt.2019.24250

160 (2019) 240–249
August

Functionalizing naturally occurring kaolinite by anatase nanoparticles and its effects on the adsorption of fluoride

Y. Han[a], S. Zhao[a,b], H. Wu[a], S. Asuha[a,b,*]

[a]*Chemistry & Environment Science College, Inner Mongolia Normal University, Inner Mongolia, 81 Zhaowudalu, Huhhot 010022, China, email: asuha@imnu.edu.cn (S. Asuha), m15848155259@163.com (Y. Han), zhaosq@imnu.edu.cn (S. Zhao), wuhs@imnu.edu.cn (H. Wu)*
[b]*Key Laboratory of Physics and Chemistry of Functional Materials, Inner Mongolia, 81 Zhaowudalu, Huhhot 010022, China*

Received 11 October 2018; Accepted 8 April 2019

ABSTRACT

The development of useful materials for removal of pollutants from water is of great importance for the world's health. In this study, naturally occurring coal-bearing kaolinite (CBK) without thermal pre-activation was successfully modified with TiO_2 by a simple one-step hydrothermal method to improve its ability to remove fluoride. The synthesized samples were characterized by X-ray diffraction analysis (XRD), N_2 adsorption-desorption analysis and transmission electron microscopy (TEM), confirming the formation of anatase nanoparticles (<10 nm) on the surface of the CBK bulk. The obtained CBK/TiO_2 nanocomposites preserved the crystalline structure of CBK and exhibited a Brunauer-Emmett-Teller (BET) surface area as high as 118.0 $m^2\ g^{-1}$. The removal efficiency of fluoride increased from 15 to 87%,when the TiO_2 content in the nanocomposite was increased from 0 to 50 mass%, indicating the fluoride-removal ability of CBK improved significantly after modification with TiO_2. The fluoride-adsorption kinetics fitted well with pseudo-second-order kinetic model, while the adsorption isotherm data could be described by either the Langmuir adsorption model or the Freundlich adsorption model. Moreover, the synthesized CBK/TiO_2 nanocomposites exhibited excellent adsorption capacities for fluoride in groundwater and it could decrease fluoride to a lesser extent (e.g., from 5.88 to 0.98 mgL^{-1}).

Keywords: Kaolinite; Modification; Titanium dioxide; Fluoride removal; Adsorption

1. Introduction

There is an increasing public concern regarding water pollution [1]. A variety of technologies have been developed to remove the pollutants from water, such as filtration, chemical precipitation, ion exchange, reverse osmosis, coagulation-flocculation and adsorption [2–7]. Among these, adsorption is believed to be the most useful method. The main advantages of adsorption are easy operation, low-cost and wide adaptability; and, thus it can be conveniently used to the treatment of many kinds of wastewater. The removal capacity, selectivity and safety of adsorption depend mainly on the properties of adsorbents. Therefore, adsorbent materials play an important role to efficiently remove pollutants from polluted water. From a viewpoint of practical use, a good adsorbent should satisfy the following two points: (i) low-cost and (ii) high removal capacity. With this in mind, the utilization of low-cost materials as a source of adsorbent is believed to be a feasible route to reduce production cost; and, hence, as low-cost adsorbents, naturally occurring clay minerals (e.g., kaolinite, bentonite and halloysite) [8–10], industrial wastes (e.g., fly ash) [11,12] and agricultural wastes [13,14] have attracted wide attention in recent years. However, it has been reported that these adsorbents suffer from low adsorption capacity due to their inactive nature and small surface area [15]. Kaolinite is one of the well-known naturally occurring clay minerals, and it is abundantly available worldwide in rocks. Therefore, it has a strong application prospect as adsorbent in water treat-

*Corresponding author.

ment. The main obstacle to the application of naturally occurring kaolinite as adsorbent is its limited adsorption capacity [9,16]. In addition, the partial Si^{4+} ions in naturally occurring kaolinite are always substituted by Al^{3+} or Fe^{3+} ions, which makes the kaolinite negatively charged. This permanent negative charge is not conducive to the adsorption of anionic pollutants on kaolinite. For this reason, the capacity of naturally occurring kaolinite for adsorption of anionic pollutants is usually smaller than that for cationic pollutants [17–20]. However, all above-mentioned disadvantages of naturally occurring kaolinite can be improved by modification, and several modification techniques have been developed for improving the activity of kaolinite, which includes milling, thermal activation and chemical activation [21–23]. Among these methods, traditional chemical activation, which mainly includes acid and alkaline treatments, is believed to be the most useful method, and thus it is widely used for activating kaolinite. Particularly, the combination of acid treatment and thermal activation can greatly increase the surface area and reactivity of kaolinite. The combination of alkaline treatment and thermal activation is also frequently used in activating kaolinite, but it does not significantly alter the surface area of kaolinite. The main disadvantage of traditional chemical activation method is to destroy the crystal structure of kaolinite. Although such an activation process can effectively improve the activity of kaolinite, but, in most cases, it completely alters the chemical composition and bulk structure of kaolinite, which is not conducive to the utilizing inherent layered structure of kaolinite for adsorption. With this in mind, surface modification techniques, such as intercalation, plasma treatment and other chemical modifications [24–27], have recently been extensively studied to modify the surface of kaolinite with preservation of the layered structure. These methods have been shown to effectively improve the reactivity of kaolinite without damaging the bulk structure. Immobilizing a functional group or active species onto the kaolinite surface is a feasible route to functionalize kaolinite. Through such a surface modification process, the surface properties of kaolinite including surface area, reactivity and sorption capacity can be greatly improved, depending on the property of immobilized species and treatment conditions. For example, organic modification can significantly improve the adsorptive removal ability of kaolinite for pollutants [28–30].

Metal oxide particles have also been proven to be promising modifiers. Especially the nanosized metal oxides are widely used for modifying many kinds of materials, since their reactivity is far higher than their bulk counterparts due to size quantization effect [31]. Therefore, another promising approach for activating clay minerals is to modify them with metal oxides nanoparticles (NPs). Anchoring metal oxides NPs onto the surface of a clay mineral not only improve the activity of clay by providing more active surface sites, but also can allow the metal oxides NPs fully display their functions by preventing particle agglomeration. Fe_2O_3, Fe_3O_4, TiO_2 and Al_2O_3 NPs are the commonly used modifiers. Particularly, the TiO_2 NPs possess excellent catalytic and adsorptive properties and are frequently used as modifiers for modifying low-cost materials to improve their removal ability for pollutants [32–35]. Despite the above reports, a study on direct modification of naturally occurring kaolinite with TiO_2 (anatase) NPs, with a detailed investigation of adsorption properties of modified kaolinite for fluoride, is rarely reported in the literature. In the present study, a naturally occurring coal-bearing kaolinite (CBK) was directly modified with anatase NPs by a novel one-step hydrothermal method, and its adsorptivities for fluoride before and after modification were investigated to explore the possibility of using CBK as a water treatment agent. CBK is an industrial solid waste generated during coal production, and thus it is expected to be a potential low-cost adsorbent used in water treatment. However, as an adsorbent for fluoride removal, it suffers from low adsorption capacity due to its small surface area and negative surface charge. To improve the adsorption ability of CBK for fluoride, we modified it using TiO_2 NPs as modifier and synthesized CBK/TiO_2 nanocomposites. The proposed method is based on the direct reaction between titanium sulfate and the naturally occurring CBK under hydrothermal condition, allowing the formation of anatase NPs on the CBK surface and the significant improvement of adsorption ability of CBK.

2. Experimental

2.1. Materials

CBK was obtained from coal mines in Inner Mongolia, northern China; and, its chemical composition (mass %) is listed as follows: SiO_2, 44.42; Al_2O_3, 39.70; Fe_2O_3, 0.22; K_2O, 0.074; MgO, 0.069; Na_2O, 0.06; CaO, 0.042; loss on ignition, 14.41. $Ti(SO_4)_2$ (98%) was purchased from Sinopharm Chemical Reagent Co., Ltd (Shanghai, China). NaF (analytical grade) was purchased from Tianjin ShengAo Chemical Reagents Co., Ltd.

2.2. Pretreatment of raw CBK

Raw CBK was mechanically crushed and sieved with 180 mesh screen (particle size < 80 μm); and then it was further grinded in a laboratory ball mill using a solid/water ratio of 1:3 (mass). The obtained CBK powder was separated from the solution and dried at 60°C.

2.3. Modification of CBK with TiO_2NPs

The pretreated CBK was modified with TiO_2 NPs as follows: 0.3 g of $Ti(SO_4)_2$ was dissolved in 20 mL of deionized water, and then 0.9 g of CBK was added to the solution under stirring. This mixture was ultrasonicated for 30 min, transferred to a stainless autoclave (50-mL) and heated at 120°C for 24 h. The obtained precipitate was separated from the solution by filtering, rinsed with deionized water several times and dried in an oven at 80°C. This produced sample with a 10 mass% TiO_2. The resulting wash liquor mixed with the solution and the obtained final solution was submitted to the measurement of dissolved Al. The samples with different TiO_2 contents up to 50 mass% were also prepared by the above method. The products are hereafter referred to as CBK/TiO_2-C in which C denote the percentage of TiO_2. For comparison, pure TiO_2 NPs were also prepared under the same conditions mentioned above.

2.4. Characterization

The phase analyses for CBK and CBK/TiO_2 nanocomposites were carried out on a Rigaku D/Max-Ultima IV X-ray diffractometer using Cu*K*α radiation (λ = 1.5418 Å) at 40 kV and 100 mA. Nitrogen gas sorption experiments were performed with a Quantachrome Instruments Autosorb-IQC analyzer with 99.999% N_2 at 77 K. Transmission electron microscopy (TEM) images were obtained on a Tecnai G2 F20 transmission electron microscope operated at 200 kV. The concentration of aluminum leached from CBK was measured using a Shimadzu ICPE-1000 atomic emission spectrometry.

2.5. Fluoride adsorption

Fluoride adsorption experiments were carried out via a batch method; and, for this, unmodified CBK, pure TiO_2 NPs and all CBK/TiO_2 nanocomposites were used as adsorbents. After adsorption, the concentration of the fluoride in the supernatant was determined by a fluoride selective electrode (Sanxin MP523, China). The calibration curve of linear relationship between standard concentration of fluoride ion and electrode potentialis shown in Fig. S1 (supplementary data).

2.5.1. Effects of contact time

100 mg of the adsorbent being tested was added to 20 mL of the 10 mg L^{-1} NaF solution; then the mixture was placed in a shaking water bath and agitated for certain time (5–120 min) at room temperature (~ 22°C). The initial pH value of the NaF solution was ~ 7.0, and it was not adjusted.

2.5.2. Effects of solution pH

In order to study the effect of solution pH on fluoride adsorption, the pH of NaF solution was adjusted from 4 to 10 using 0.1 M NaOH or HCl solutions prior to adsorption test. The adsorbent dose, volume of NaF solution, concentration of NaF solution, contact time and temperature were set at 100 mg, 20 mL, 10 mg L^{-1}, 60 min and 22°C, respectively.

2.5.3. Effects of initial NaF concentration

Adsorption experiments were carried out on various initial NaF concentrations (5–50 mg L^{-1})to study the effect of initial NaF concentration on fluoride adsorption. For this, the adsorbent dose, volume of NaF solution, contact time and temperature were set at 100 mg, 20 mL, 60 min and 22°C, respectively. The pH of solution was close to 7.0, and it was not further adjusted.

2.5.4. Adsorption of fluoride from groundwater

To further investigate the adsorption performance of synthesized materials for water containing naturally excess of fluoride, adsorption tests were carried out using an actual groundwater. For this, a groundwater sample was collected from Xilingol, a typical high fluorine area of Inner Mongolia. The F^- concentration and pH of the sample were 5.88 mg L^{-1} and 8.4, respectively. Before adsorption test, the pH of the water sample was adjusted to 7.0 using 0.1 M HCl; and, the adsorbent dose, volume of solution, contact time and temperature were set at 100 mg, 20 mL, 60 min and 22°C, respectively.

3. Results and discussion

3.1. Modification of CBK with TiO_2NPs

The procedure adopted for the modification of CBK with TiO_2 NPs is illustrated in Fig. 1, which is based on the ability of $Ti(SO_4)_2$to directly react with CBK without thermal pre-activation and to be transformed into TiO_2 NPs under one-step hydrothermal reaction condition. The following three chemical processes are thought to take place during the hydrothermal treatment: (i) hydrolysis of $Ti(SO_4)_2$ to form sulfuric acid, (ii) reaction of sulfuric acid with CBK and (iii) formation of TiO_2 nanoparticles on the CBK surface. According to previous study, sulfuric acid can directly react with aluminum in CBK at an elevated temperature [36]. Therefore, the sulfuric acid produced in the first process causes the dissolution of Al^{3+} cations from the octahedral sheet of kaolinite in the second process, which results in the formation of porous surface layer and thus allows for the loading of a large amount of Ti^{4+} ions. Third chemical process mainly includes the hydrolysis of the Ti^{4+} ions loaded in the porous skeleton of CBK and the formation of TiO_2 NPs. Fig. 2 shows the XRD patterns of CBK, $TiO_2$and the CBK/TiO_2 nanocomposites. All reflections observed in the XRD pattern of original CBK matched well with the JCPDS file (e.g., No. 14-0164) of kaolinite, and those observed in XRD pattern of synthesized pure TiO_2 were in good agreement with the JCPDS file (e.g., No.71-1167) of anatase. Comparing the XRD patterns of CBK, TiO_2 and CBK/TiO_2 nanocompos-

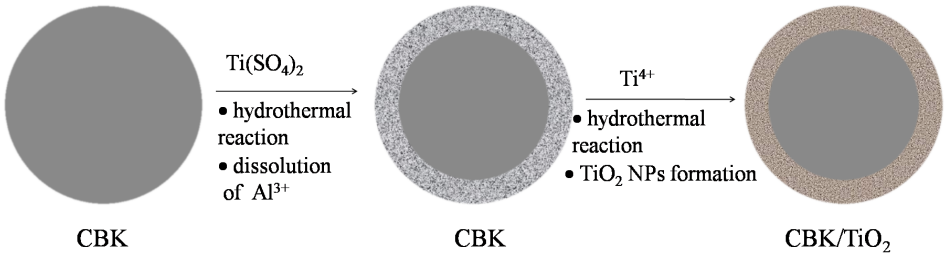

Fig. 1. Schematic illustration for the direct modification of CBK with TiO_2 NPs.

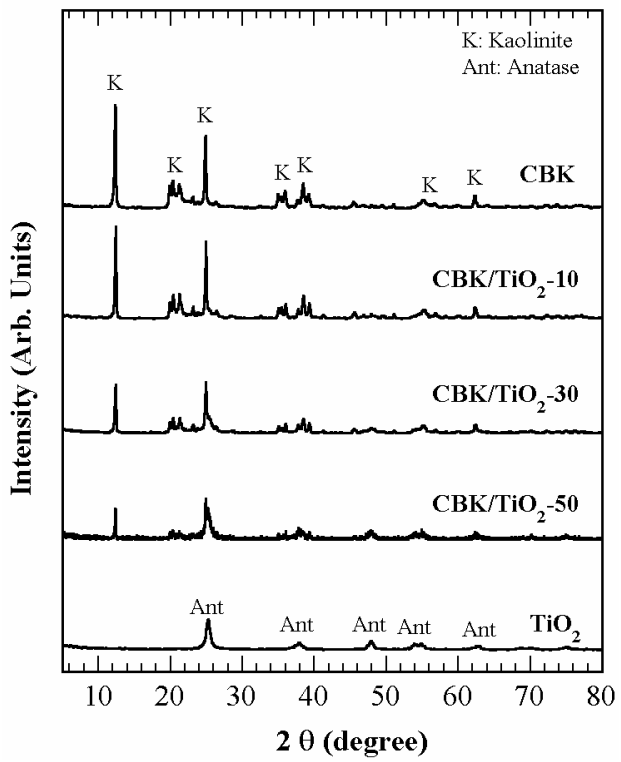

Fig. 2. XRD patterns of CBK, TiO_2 and CBK/TiO_2.

ites, it was found that the reflections of both CBK and pure TiO_2 appeared in the patterns of all synthesized CBK/TiO_2 nanocomposites, and the intensities of main reflections of kaolinite and anatase depended on the TiO_2 content in the nanocomposite. As the TiO_2 content was increased from 10 to 50%, the reflections of kaolinite progressively weakened while the intensity of anatase peaks gradually increased. These results indicated the following: (i) the crystalline structure of kaolinite was retained in the all CBK/TiO_2 nanocomposites and (ii) the formation of anatase phase in all CBK/TiO_2 samples, proving that the nanocomposites were composed of kaolinite and anatase. For CBK/TiO_2 nanocomposites, as seen in the figure, the main reflections of anatase overlapped with those of kaolinite, which makes it difficult to estimate the average crystallite size of TiO_2 NPs from their XRD patterns. The average crystallite size of pure TiO_2 NPs was estimated to be 10.2 nm, using Scherrer's equation. This suggest that the average crystallite size of TiO_2 NPs in the CBK/TiO_2 nanocomposites was smaller than 10 nm, since the intensities of diffraction peaks TiO_2 in CBK/TiO_2 composites were obviously weaker than that of pure TiO_2. Fig. 3 shows TEM images of CBK and CBK/TiO_2 nanocomposites. The naturally occurring CBK consisted only of large particles (Fig. 3a). In contrast, numerous small particles (TiO_2) were found in the images of CBK/TiO_2 nanocomposites and they were randomly dispersed over the CBK support (Figs. 3b, c, d). In addition, the amount of TiO_2 particles increased with the increase of TiO_2 content in the composite. High-resolution

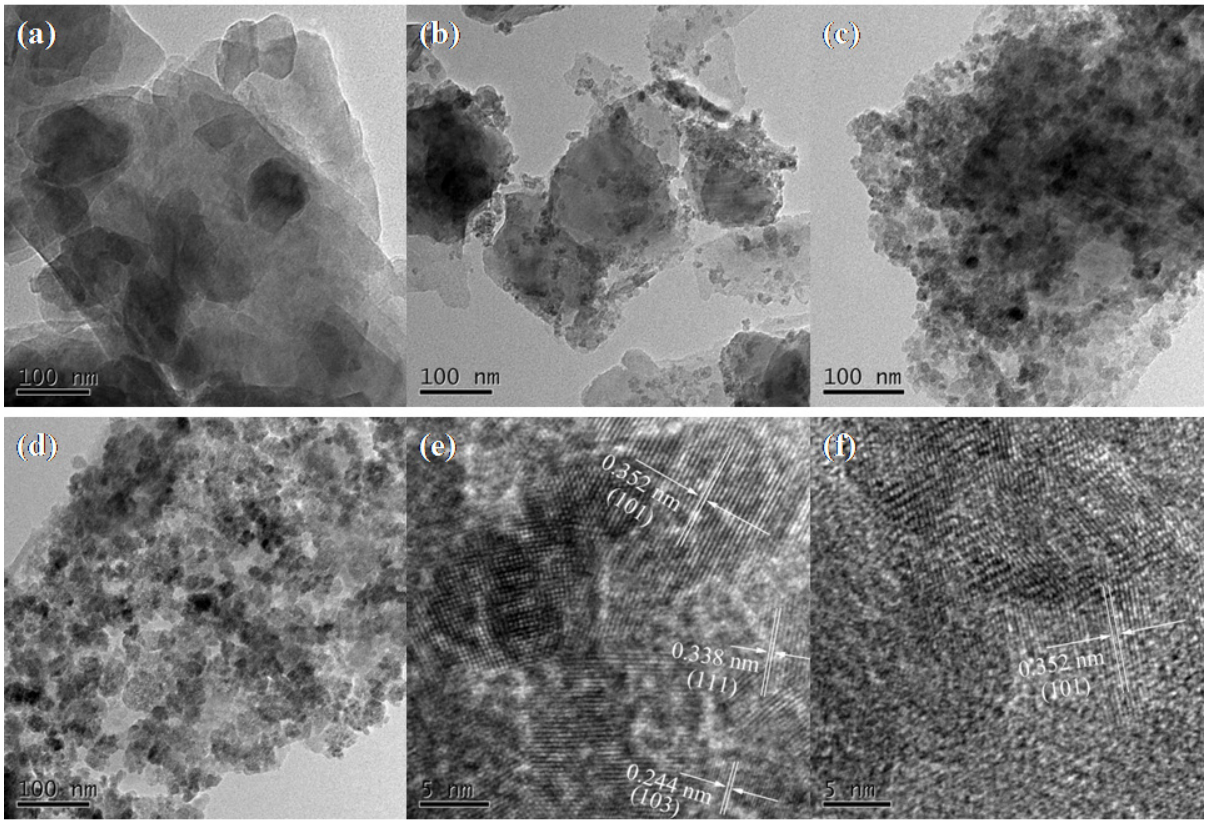

Fig. 3. TEM images of CBK (a), CBK/TiO_2-10 (b), CBK/TiO_2-30 (c, e) and CBK/TiO_2-50 (d, f).

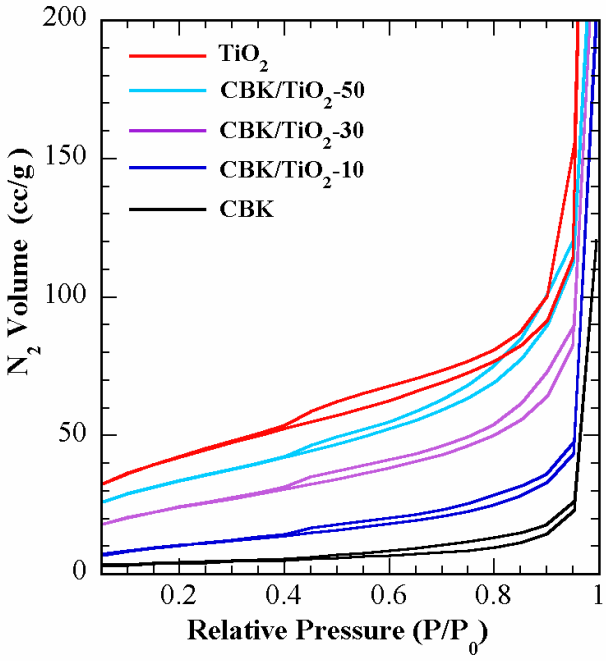

Fig. 4. N_2 adsorption-desorption isotherms of CBK, TiO_2 and CBK/TiO_2.

TEM (HRTEM) images of nanocomposites revealed that the TiO_2 NPs were highly crystalline, with their atomic lattice fringes being clearly seen in the image with interplanar spacing of 0.352 nm for (101) plane, 0.338 nm for (111) plane and 0.244 nm for (103) plane (Figs. 3e, f) of anatase. The HRTEM images also shown that the crystallite sizes of TiO_2 NPs in the samples CBK/TiO_2-30 and CBK/TiO_2-50 were less than 10 nm, which agreed with the result obtained by XRD analysis.

Fig.4 shows the N_2 adsorption-desorption isotherms of CBK, TiO_2 and CBK/TiO_2 nanocomposites. The BET surface areas, average pore diameters and specific pore volumes of the samples are given in Table 1. According to the IUPAC classification, the isotherm of original CBK was in keeping with a type II isotherm, indicating that the CBK was anon-porous aggregate [37]. After modification with TiO_2, the isotherm of CBK changed greatly along with the increase of TiO_2 content in the CBK/TiO_2 nanocomposite. When the TiO_2 content increased from 0 to 50%, the sorption quantity of N_2 on resulting sample increased progressively. At the same time, the shape of isotherm became close to a type IV isotherm, indicating that the non-porous CBK has been transformed into mesoporous one. As a result, the BET surface area of CBK increased from 21.2 to 118.0 $m^2\ g^{-1}$ when the content of loaded TiO_2 increased from 0 to 50%. This increase in the surface area may be due to the following two reasons: (i) dissolution of Al^{3+} from the CBK and (ii) increase of new surface. As mentioned earlier, the sulfuric acid produced via the hydrolysis of $Ti(SO_4)_2$ can directly react with CBK and causes the dissolution of Al^{3+} cations under hydrothermal condition:

$$Ti(SO_4)_2 + 4H_2O \rightarrow 2H_2SO_4 + Ti^{4+} + 4OH^- \quad (1)$$

$$Al_2O_3{\cdot}2SiO_2{\cdot}2H_2O + 3H_2SO_4 \rightarrow Al_2(SO_4)_3 + 2SiO_2 + 5H_2O \quad (2)$$

Table 1
Textural properties of the studied samples

Sample	BET surface area ($m^2\ g^{-1}$)	V_s [a] ($cm^3\ g^{-1}$)	P_d [b] (nm)
CBK	21.2	0.07	30.7
CBK/TiO_2-10	39.0	0.30	3.41
CBK/TiO_2-30	85.5	0.35	3.42
CBK/TiO_2-50	118.0	0.37	3.42
TiO_2	147.8	0.64	3.41

[a]V_s = specific pore volume at P/P_0 = 0.97.
[b]P_d = average pore diameter.

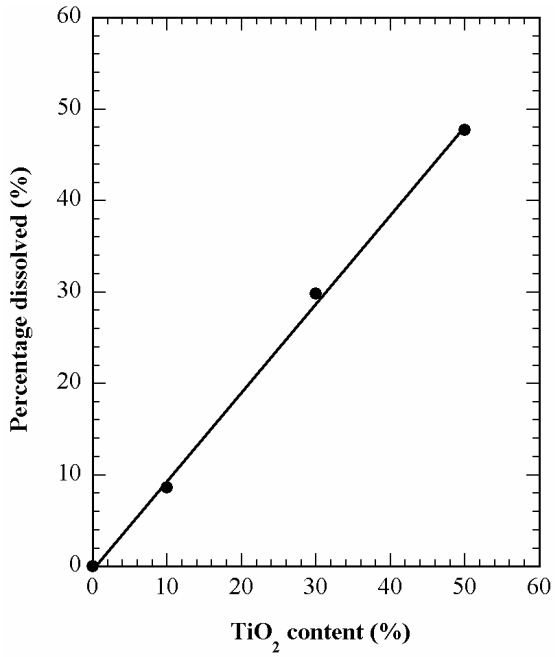

Fig. 5. Al dissolution as a function of TiO_2 content in CBK/TiO_2.

To confirm this, we measured the amount of leached Al^{3+} and found that the percentage of dissolved Al^{3+} increases monotonously with the increase of $Ti(SO_4)_2$/CBK ratio (or TiO_2 content in the TiO_2/CBK nanocomposite) (Fig. 5). The leaching of Al^{3+} cations from kaolinite would results in the formation of mesopores and/or micropores, which can effectively increase the surface area of CBK [36]. In addition, the formation of TiO_2 NPs on the surface of CBK also can increase the surface area by creating new surface, due to their large surface area to volume ratio.

3.2. Adsorption properties

3.2.1. Adsorption kinetics

Fig. 6 shows the adsorption rate curves and pseudo-second-order kinetics plots for the adsorption of fluoride on CBK, TiO_2 and CBK/TiO_2 nanocomposites. For all samples, the adsorption reached equilibrium within 20 min, indicating that the adsorption kinetics of the fluoride were very

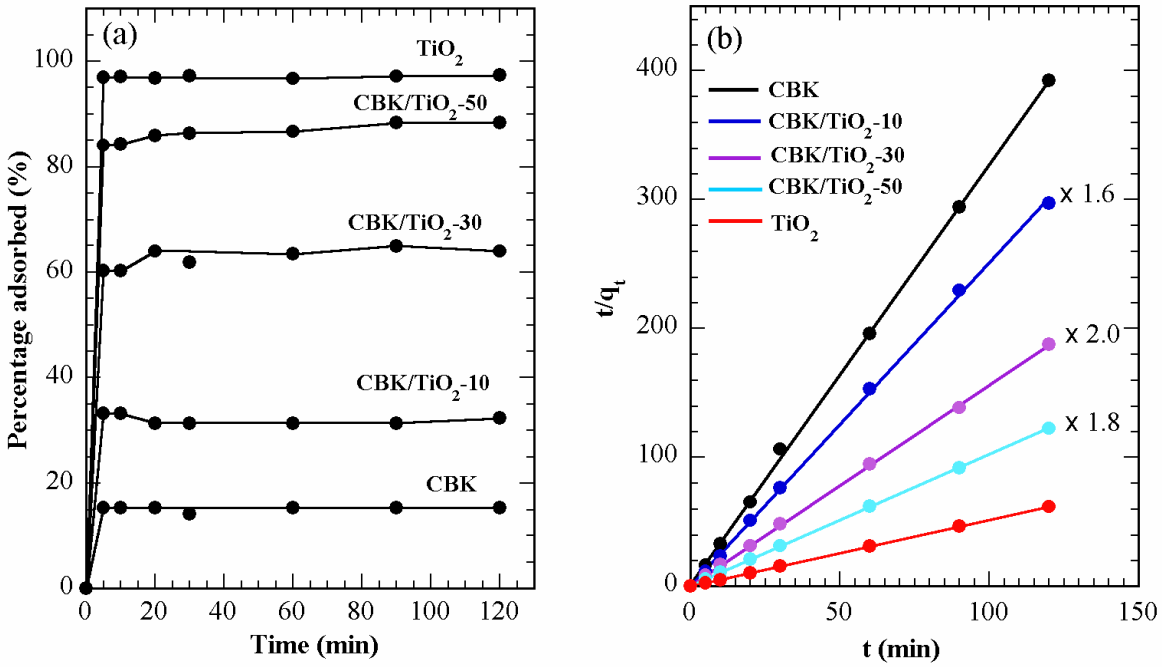

Fig. 6. Adsorption rate curves (a) and pseudo-second-order adsorption kinetics (b) of fluoride on CBK, TiO_2 and CBK/TiO_2.

fast (Fig. 6a). Of all the investigated samples, pristine CBK exhibited the lowest adsorption efficiency (~15%) for fluoride. In contrast, the TiO_2 NPs showed a highest adsorption efficiency of 98%. Owing to the high adsorption ability of TiO_2 NPs for fluoride, the fluoride-removing efficiency of CBK increased largely after the loading of TiO_2 NPs, indicating that the removal abilities of naturally occurring CBK for fluoride can be significantly improved by modifying it with TiO_2 NPs. The result can be explained from the properties of adsorbents and the adsorbate. The BET surface area of TiO_2 NPs was about 7 times larger than that of CBK. This may be the probable main reason for the difference in the adsorption abilities of these two adsorbents, since the adsorptive active sites of an adsorbent are always proportional to its surface area [38,39]. On the other hand, the fluoride adsorption also depend on the existence form of F in aqueous solution. When the NaF is dissolved in water, the F is mainly present in the forms of F^- or HF, according to the following hydrolysis reaction of NaF:

$$NaF + H_2O \rightleftharpoons HF + NaOH \quad (3)$$

$$HF \rightleftharpoons H^+ + F^- \quad (4)$$

As mentioned earlier, the CBK has a permanent negative charge. Therefore, the electrostatic repulsion between negatively charged F^- and CBK inhibits fluoride adsorption. In the case of TiO_2 NPs, however, they were formed via the hydrolysis of $Ti(SO_4)_2$, which not only produced TiO_2 NPs, but also yielded sulfuric acid, according to Eq. (1). Under such acidic conditions, the surface hydroxyl groups of TiO_2 NPs will react with H^+ ions and form positively charged $TiOH_2^+$, which increases the affinity to negatively charged F^- ions.

The fluoride adsorption data were fitted to pseudo-first-order and pseudo-second-order kinetic models using the following equations [40]:

$$\log(q_e - q_t) = \log q_e - \frac{k_1}{2.303}t \quad (5)$$

$$\frac{t}{q_t} = \frac{1}{k_2 q_e^2} + \frac{t}{q_e} \quad (6)$$

where q_t (mg g^{-1}) and q_e (mg g^{-1}) are the amounts of fluoride adsorbed at time t (min) and at equilibrium, respectively, and k_1 (min^{-1}) and k_2 (g mg^{-1} min^{-1}) are the first-order and second-order kinetic rate constants, respectively. The fitting results are shown in Table 2. For all samples, the R^2 values of the pseudo-first-order model were lower than those of the pseudo-second-order model. Further, the $q_{e,cal}$ values of the pseudo-first-order model did not agree with the experimental q_e value. In contrast, the R^2 values of the pseudo-second-order model were higher than 0.999 for all samples; and, thus the plots t/q_t versus t were straight lines in all the cases (Fig. 6b). Further, the $q_{e,cal}$ values obtained using this model were closer to the experimental q_e values, indicating that the adsorption of fluoride on studied samples followed the pseudo-second-order model.

3.2.2. Effects of solution pH

In general, the solution pH has a significant effect on adsorption. Particularly, the adsorption of anionic and cationic pollutants depends strongly on the solution pH, and an acidic condition is ideal for anionic pollutant adsorption when a clay mineral or metal oxide is used as the adsorbent. This trend was observed in the present study, too. Fig. 7 shows

Table 2
Kinetic parameters for the adsorption of fluoride on CBK, CBK/TiO_2 and TiO_2 NPs

Adsorbent	C_0	$q_{e,exp}$	Pseudo-first order-model			Pseudo-second order-model		
	(mg L^{-1})	(mg g^{-1})	k_1 (min^{-1})	$q_{e,cal}$ (mg g^{-1})	R^2	k_2 (g mg^{-1} min^{-1})	$q_{e,cal}$ (mg g^{-1})	R^2
CBK	10	0.31	–	–	–	7.91	0.31	0.9995
CBK/TiO_2-10	10	0.68	0.017	0.22	0.2828	11.63	0.64	0.9994
CBK/TiO_2-30	10	1.30	0.02	0.14	0.2716	1.74	1.29	0.9998
CBK/TiO_2-50	10	1.77	0.04	0.20	0.3452	1.23	1.77	1.0000
TiO_2	10	1.95	0.025	0.029	0.0042	8.12	1.94	1.0000

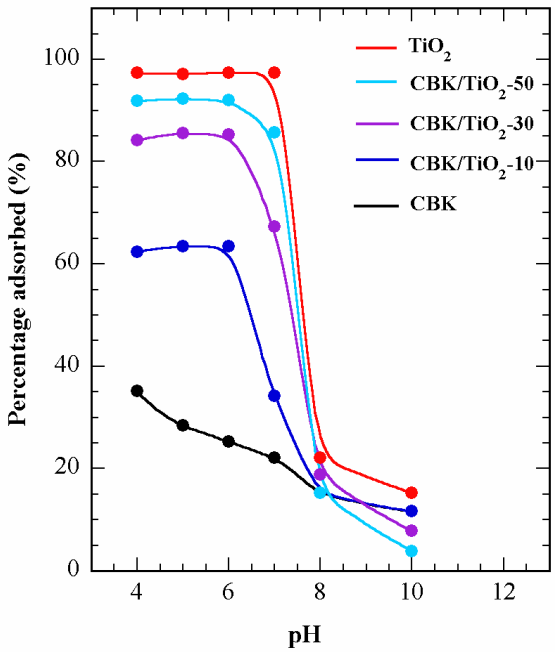

Fig. 7. Influence of solution pH on adsorption of fluoride on CBK, TiO_2 and CBK/TiO_2.

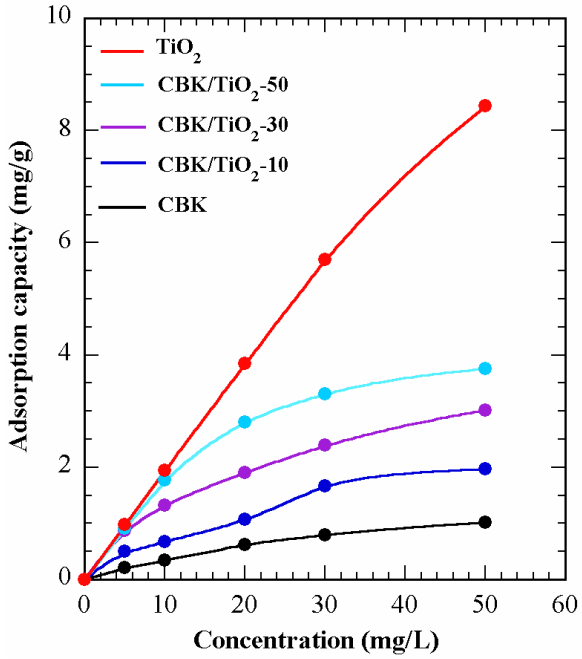

Fig. 8. Adsorption isotherms of fluoride on CBK, TiO_2 and CBK/TiO_2.

the effects of the solution pH on the fluoride-removal abilities of CBK, TiO_2 and CBK/TiO_2 nanocomposites. For all samples, the adsorbed percentages of fluoride at acidic pH were higher than those at basic pH, mainly due to the electrostatic attraction between negatively charged F^- and positively charged adsorbent surface under acidic condition. In addition, the removal efficiencies of fluoride on CBK/TiO_2 nanocomposites were found to be larger than that on unmodified CBK in the pH range from 4 to 8 and increased with the increase of TiO_2 content, showing that modified CBK had much adsorption abilities than unmodified CBK. Under alkaline conditions, the surface hydroxyl groups of TiO_2 NPs will be dissociated to form TiO^-, i.e., TiO_2 surface will be negatively charged; consequently, the electrostatic repulsion between negatively charged F^- and TiO_2 surface inhibits adsorption.

3.2.3. Adsorption isotherms

The adsorption isotherms of fluoride for CBK, TiO_2 and CBK/TiO_2 nanocomposites are shown in Fig. 8. The adsorption capacities of CBK/TiO_2 nanocomposites for fluoride in all studied initial concentration range obviously increased with increasing TiO_2 content in the composites. The following Langmuir and Freundlich equations were employed to fit the experimental data.

$$\frac{C_e}{q_e} = \frac{1}{K_L q_m} + \frac{C_e}{q_m} \tag{7}$$

$$\ln q_e = \ln K_F + \frac{1}{n} \ln C_e \tag{8}$$

where C_e (mg L^{-1}) is the equilibrium concentration of the fluoride, q_e (mg g^{-1}) is the equilibrium adsorption capacity, K_L (L mg^{-1}) is the Langmuir equilibrium constant, q_m (mg g^{-1}) is the maximum monolayer adsorption capacity, K_F is the Freundlich adsorption equilibrium constant and n is the Freundlich intensity factor. The result of data fitting is listed in Table 3. The fluoride adsorption data fitted well with either the Langmuir or the Freundlich adsorption model. The Freundlich constant n was larger than 1 for all samples, showing the favorable adsorption of fluoride. Fluoride is

Table 3
Langmuir and Freundlich isotherm parameters for the adsorption of fluoride on CBK, CBK/TiO_2 and TiO_2 NPs

Adsorbent	Langmuir model			Freundlich model		
	q_m (mg g^{-1})	K_L (L mg^{-1})	R^2	K_F	n	R^2
CBK	1.4	0.039	0.9471	0.09	1.63	0.9815
CBK/TiO_2-10	2.85	−0.048	0.7493	0.27	1.92	0.9093
CBK/TiO_2-30	3.06	0.18	0.8968	0.91	3.40	0.9508
CBK/TiO_2-50	3.67	0.64	0.9986	1.38	3.17	0.9067
TiO_2	10.09	0.80	0.9977	3.63	1.85	0.9420

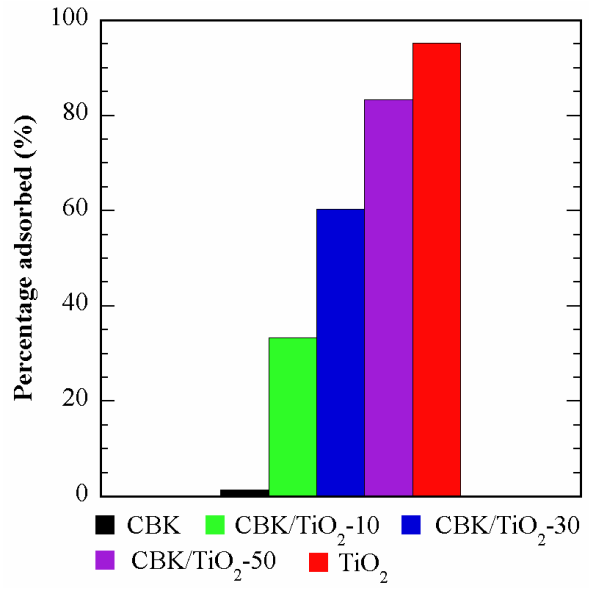

Fig. 9. Adsorption efficiency of fluoride in groundwater.

adsorbed on the surface of adsorbents mainly by means of electrostatic attraction and hydrogen bond formation at the low pH condition. Therefore, the presence of multiple adsorption sites may be the most probable reason for well fit with Langmuir and the Freundlich adsorption models.

3.2.4. Adsorption of fluoride from groundwater

Fig. 9 shows the degrees of adsorption of fluoride from an actual groundwater containing 5.88 mg L^{-1} F^- ions. The F^- concentrations in groundwater after treatment are listed in Table 4. As shown in Fig. 9, the adsorption efficiency of F^- ions on pristine CBK was as low as 1.4 %. After modification with TiO_2 NPs, the F-removing efficiency of CBK increased markedly and was proportional to the TiO_2 content in the CBK/TiO_2 nanocomposites; and, for CBK/TiO_2-50 sample, it reached as high as 83.4%. Among all studied samples, the-TiO_2 NPs still showed the highest removal ability (95.2%). The F^- concentration in groundwater adsorbed with CBK/TiO_2-50 and pristine TiO_2 NPs were reduced to 0.98 and 0.28 mg L^{-1}, respectively. These values are far lower than the maximum permissible limit (1.5 mg L^{-1}) for drinking water recommended by World Health Organization (WHO) [41].

Table 4
F concentration in treated groundwater

Adsorbent	F concentration (mg L^{-1})
CBK	5.80
CBK/TiO_2-10	3.92
CBK/TiO_2-30	2.33
CBK/TiO_2-50	0.98
TiO_2	0.28

4. Conclusions

Direct reaction between titanium sulfate and naturally occurring CBK under hydrothermal condition led to the formation of TiO_2 NPs on the surface of the CBK bulk, resulting in the formation of CBK/TiO_2 nanocomposite. After modification with TiO_2, the both BET surface area and specific pore volume of CBK increased greatly along with the increase of TiO_2 content in the CBK/TiO_2 nanocomposite. Compared to unmodified CBK, the CBK/TiO_2 nanocomposites exhibited much greater adsorption capacities for fluoride, and the fluoride-removal efficiency increased with an increase in the TiO_2 content, suggesting that the fluoride-removal capacity of naturally occurring CBK can be significantly improved by modification with TiO_2. Further, the adsorption rate of fluoride on CBK/TiO_2 nanocomposites was very fast and reached adsorption equilibrium within 20 min, and its adsorption kinetics fitted well with the pseudo-second-order kinetic model. The adsorptivity of the CBK/TiO_2 nanocomposites for fluoride depended significantly on the solution pH, with acidic conditions increasing the adsorption.

Acknowledgments

This work was supported by National Natural Science Foundation of China (Grant Nos. 21267016), and Program for Inner Mongolia Excellence Specialist.

References

[1] A. Subramani, J.G. Jacangelo, Emerging desalination technologies for water treatment: A critical review, Water Res., 75 (2015) 164–187.

[2] A.K.A. Ahmed, T.F. Marhaba, Review on river bank filtration as an in situ water treatment process, Clean Technol. Environ., 19 (2017) 349–359.
[3] P.M. Melia, A.B. Cundy, S.P. Sohi, P.S. Hooda, R. Busquets, Trends in the recovery of phosphorus in bioavailable forms from wastewater, Chemosphere, 186 (2017) 381–395.
[4] I. Levchuk, J.J. Rueda Márquez, M. Sillanpää, Removal of natural organic matter (NOM) from water by ion exchange – A review, Chemosphere, 192 (2018) 90–104.
[5] H. Lee, Y. Jin, S. Hong, Recent transitions in ultrapure water (UPW) technology: Rising role of reverse osmosis (RO), Desalination, 399 (2016) 185–197.
[6] P. Das, M.I. Thaher, M.A.Q.M. Abdul Hakim, H.M.S.J. Al-Jabri, G.S.H.S. Alghasal, Microalgae harvesting by pH adjusted coagulation-flocculation, recycling of the coagulant and the growth media, Bioresour. Technol., 216 (2016) 824–829.
[7] I. Ali, New generation adsorbents for water treatment, Chem. Rev., 112 (2012) 5073–5091.
[8] T. Ngulube, J.R. Gumbo, V. Masindi, A. Maity, An update on synthetic dyes adsorption onto clay based minerals: A state-of-art review, J. Environ. Manage., 191 (2017) 35–57.
[9] M. Rafatullah, O. Sulaiman, R. Hashim, A. Ahmad, Adsorption of methylene blue on low-cost adsorbents: A review, J. Hazard. Mater., 177 (2010) 70–80.
[10] M.K. Uddin,A review on the adsorption of heavy metals by clay minerals, with special focus on the past decade, Chem. Eng. J., 308 (2017) 438–462.
[11] C. An, S. Yang, G. Huang, S. Zhao, P. Zhang, Y. Yao, Removal of sulfonated humic acid from aqueous phase by modified coal fly ash waste: Equilibrium and kinetic adsorption studies, Fuel, 165 (2016) 264–271.
[12] M. Visa, L. Andronic, A. Enesca, Behavior of the new composites obtained from fly ash and titanium dioxide in removing of the pollutants from wastewater, Appl. Surf. Sci., 388 (2016) 359–369.
[13] E. Rosales, J. Meijide, M. Pazos, M.A. Sanromán, Challenges and recent advances in biochar as low-cost biosorbent: From batch assays to continuous-flow systems, Bioresour. Technol., 246 (2017) 176–192.
[14] B. Saba, A.D. Christy, M. Jabeen, Kinetic and enzymatic decolorization of industrial dyes utilizing plant-based biosorbents: A review, Environ. Eng. Sci., 33 (2016) 601–614.
[15] I. Ali, M. Asim, T.A. Khan, Low cost adsorbents for the removal of organic pollutants from wastewater, J. Environ. Manage., 113 (2012) 170–183.
[16] M. Jiang, Q. Wang, X. Jin, Z. Chen, Removal of Pb(II) from aqueous solution using modified and unmodified kaolinite clay, J. Hazard. Mater., 170 (2009) 332–339.
[17] W. Hajjaji, A. Kovicova, R.C. Pullar, D.M. Tobaldi, A. Lopez-Galindo, F. Jammousi, F. Rocha, J.A. Labrincha, Effective removal of anionic and cationic dyes by kaolinite and TiO_2/kaolinite composites, Clay Miner., 51 (2016) 19–27.
[18] A.R. Tehrani-Bagha, H. Nikkar, N.M. Mahmoodi, M. Markazi, F.M. Menger, The sorption of cationic dyes onto kaolin: Kinetic, isotherm and thermodynamic studies, Desalination, 266 (2011) 274–280.
[19] V. Vimonses, S. Lei, B. Jin, C.W.K. Chow, C. Saint, Adsorption of Congo red by three Australian kaolins, Appl. Clay Sci., 43 (2009) 465–472.
[20] B.K. Nandi, A. Goswami, M.K. Purkait, Removal of cationic dyes from aqueous solutions by kaolin: Kinetic and equilibrium studies, Appl. Clay Sci., 42 (2009) 583–590.
[21] É. Makó, Z. Senkár, J. Kristóf, V. Vágvölgyi, Surface modification of mechanochemically activated kaolinites by selective leaching, J. Colloid Interface Sci., 294 (2006) 362–370.
[22] C. Belver, M.A.B. Munoz, M.A. Vicente, Chemical activation of a kaolinite under acid and alkaline conditions, Chem. Mater., 14 (2002) 2033–2043.
[23] P.E.A. Lima, R.S. Angélica, R.F. Neves, Dissolution kinetics of metakaolin in sulfuric acid: Comparison between heterogeneous and homogeneous reaction methods, Appl. Clay Sci., 88–89 (2014) 159–162.
[24] H. Cheng, Q. Liu, X. Cui, Q. Zhang, Z. Zhang, R.L. Frost, Mechanism of dehydroxylation temperature decrease and high temperature phase transition of coal-bearing strata kaolinite intercalated by potassium acetate, J. Colloid Interface Sci., 376 (2012) 47–56.
[25] T. Yavuz, C. Saka, Surface modification with cold plasma application on kaolin and its effects on the adsorption of methylene blue, Appl. Clay Sci., 85 (2013) 96–102.
[26] M. Khairy, H.A. Ayoub, F.A. Rashwan, H.F. Abdel-Hafez, Chemical modification of commercial kaolin for mitigation of organic pollutants in environment via adsorption and generation of inorganic pesticides, Appl. Clay Sci., 153 (2018) 124–133.
[27] M. Al-Harahsheh, R. Shawabkeh, A. Al-Harahsheh, K. Tarawneh, M.M. Batiha, Surface modification and characterization of Jordanian kaolinite: Application for lead removal from aqueous solutions, Appl. Surf. Sci., 255 (2009) 8098–8103.
[28] Y. Chen, D. Lu, Amine modification on kaolinites to enhance CO_2 adsorption, J. Colloid Interface Sci., 436 (2014) 47–51.
[29] U.F. Alkaram, A.A. Mukhlis, A.H. Al-Dujaili, The removal of phenol from aqueous solutions by adsorption using surfactant-modified bentonite and kaolinite, J. Hazard. Mater., 169 (2009) 324–332.
[30] Q. Zhang, Z. Yan, J. Ouyang, Y. Zhang, H. Yang, D. Chen, Chemically modified kaolinite nanolayers for the removal of organic pollutants, Appl. Clay Sci., 157 (2018) 283–290.
[31] C. Santhosh, V. Velmurugan, G. Jacob, S.K. Jeong, A.N. Grace, A. Bhatnagar, Role of nanomaterials in water treatment applications: A review, Chem. Eng. J., 306 (2016) 1116–1137.
[32] Z. Lu, W. Zhou, P. Huo, Y. Luo, M. He, J. Pan, C. Li, Y. Yan, Performance of a novel TiO_2 photocatalyst based on the magnetic floating fly-ash cenospheres for the purpose of treating waste by waste, Chem. Eng. J., 225 (2013) 34–42.
[33] Y. Hai, X. Li, H. Wu, S. Zhao, W. Deligeer, S. Asuha, Modification of acid-activated kaolinite with TiO_2 and its use for the removal of azo dyes, Appl. Clay Sci., 114 (2015) 558–567.
[34] X.F. Chen, S.R. Lin, S.C. Kou, Effect of composite photo-catalysts prepared with recycled clay brick sands and nano-TiO_2 on methyl orange and NOx removal, Constr. Build. Mater., 171 (2018) 152–160.
[35] L. Yang, C. Wang, Z. Liu, X. Liu, Y. Song, X. Feng, B. Zhang, Functionalizing slag wool fibers with photocatalytic activity by anatase TiO_2 and CTAB modification, Ceram. Int., 44 (2018) 5842–5847.
[36] W. Gao, S. Zhao, H. Wu, W. Deligeer, S. Asuha, Direct acid activation of kaolinite and its effects on the adsorption of methylene blue, Appl. Clay Sci., 126 (2016) 98–106.
[37] K.S.W. Sing, D.H. Everett, R.A.W. Haul, L. Moscou, R.A. Pierotti, J. Rouquérol, T. Siemieniewska, Reporting physisorption data for gas/solid systems-with special reference to the determination of surface area and porosity, Pure Appl. Chem., 57 (1985) 603–619.
[38] J. Shen, J. Sulkowski, M. Beckner, A. Dailly, Effects of textural and surface characteristics of metal-organic frameworks on the methane adsorption for natural gas vehicular application, Micropor. Mesopor. Mater., 212 (2015) 80–90.
[39] N. Hegyesi, R.T. Vad, B. Pukánszky, Determination of the specific surface area of layered silicates by methyleneblue adsorption: The role of structure, pH and layer charge, Appl. Clay Sci., 146 (2017) 50–55.
[40] Y.S. Ho, G. McKay, Pseudo-second order model for sorption processes, Process Biochem., 34 (1999) 451–465.
[41] L.H. Velazquez-Jimenez, E. Vences-Alvarez, J.L. Flores-Arciniega, H. Flores-Zuniga, J.R. Rangel-Mendez, Water defluoridation with special emphasis on adsorbents-containing metal oxides and/or hydroxides: A review, Sep. Purif. Technol., 150 (2015) 292–307.

Supporting information

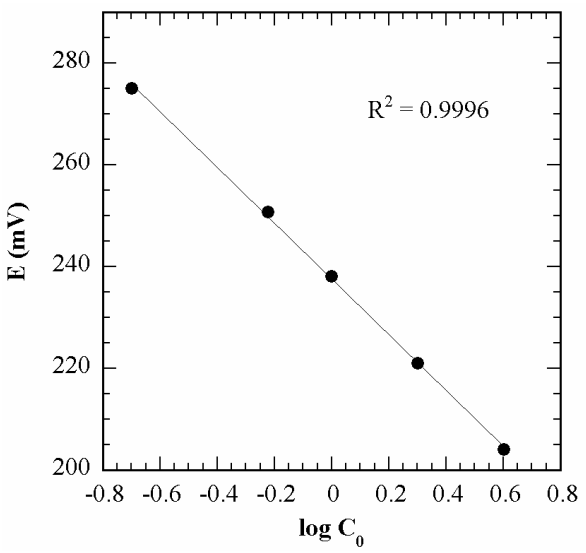

Fig. S1. Standard curve for determination of fluoride ion concentration.